
Article:
Paul, M., Peckelsen, K., Thomulka, T. et al. (7 more authors) (2019) Hydrogen tunneling avoided : enol-formation from a charge-tagged phenyl pyruvic acid derivative evidenced by tandem-MS, IR ion spectroscopy and theory. Physical Chemistry Chemical Physics, 21 (30). pp. 16591-16600. ISSN 1463-9076

https://doi.org/10.1039/c9cp02316j

Hydrogen Tunneling Avoided: Enol-Formation From a Charge-tagged Phenyl Pyruvic Acid Derivative Evidenced by Tandem-MS, IR Ion Spectroscopy and Theory

Mathias Paul,[1] Katrin Peckelsen,[1] Thomas Thomulka,[1] Jörg Neudörfl,[1] Jonathan Martens,[2] Giel Berden,[2]Jos Oomens,[2,3] Albrecht Berkessel,[1] Anthony J. H. M. Meijer*,[4] and Mathias Schäfer*,[1]

[1] University of Cologne, Department of Chemistry, Greinstrasse 4, 50939 Köln, Germany.
[2] Radboud University, Institute for Molecules and Materials, FELIX Laboratory, Toernooiveld 7c, 6525 ED Nijmegen, The Netherlands.
[3] Van't Hoff Institute for Molecular Sciences, University of Amsterdam, Science Park 904, 1098 XH Amsterdam, The Netherlands.
[4] University of Sheffield, Department of Chemistry, Sheffield S3 7HF, U.K.

Abstract

A charge-tagged phenyl pyruvic acid derivative was investigated by tandem-MS, infrared (IR) ion spectroscopy and theory. The tailor-made precursor ions efficiently lose CO_2 in collision induced dissociation (CID) experiments, offering access to study the secondary decay reactions of the product ions. IR ion spectroscopy provides evidence for the formation of an enol acid precursor ion structure in the gas phase and indicates the presence of enol products formed after CO_2 loss. Extensive DFT computations however, suggest intermediate generation of hydroxycarbene products, which in turn rearrange in a secondary process to the enol ions detected by IR ion spectroscopy. Quantum mechanical tunneling of the hydroxycarbene can be excluded since no evidence for aldehyde product ion formation could be found. This finding is in contrast to the behavior of methylhydroxycarbene, which cleanly penetrates the energy barrier to form exclusively acetaldehyde at cryogenic temperatures in an argon matrix via quantum mechanical hydrogen tunneling. The results presented here are attributed to the highly excited energy levels of the product ions formed by CID in combination with different barrier heights of the competing reaction channels, which allow exclusive access *over* one energy barrier leading to the formation of the enol tautomer ions observed.

1. Introduction

Carbenes are divalent carbon atoms with special reactivity features that include umpolung, the reaction concept that underlies major enzymatic transformations in biochemistry and is of fundamental importance for organocatalysis, *e.g.* the carbene-catalyzed benzoin-condensation.[1-4] Methylhydroxycarbene (**1**), as shown in Scheme 1, is a highly reactive and delicate singlet carbene, which offers a nucleophilic electron pair as well as an empty orbital for polar intra- or intermolecular interactions rendering isolation and characterization difficult.[6] Adapted from enzymology, Schreiner et al. have demonstrated in a series of contributions that α-ketocarboxylic acids such as pyruvic, glyoxylic and, phenylglyoxylic acid can serve as effective hydroxycarbene precursors, when introduced to high-vacuum flash pyrolysis (HVFP) in which they lose CO_2 effectively.[1,3,6-10] Trapping of the respective pyrolysis products in solid noble gas matrices at cryogenic temperatures allowed the spectroscopic characterization of a broad variety of hydroxycarbenes by absorption spectroscopy. IR spectroscopy along with high-level computations showed that the clean [1,2]H-shift reaction of hydroxycarbenes to respective tautomers observed at 11 K is actually a quantum-mechanical hydrogen tunneling process.[6-10] Specifically, methylhydroxycarbene (**1**) delivers acetaldehyde, and not vinyl alcohol by penetration of the higher, but narrower energy barrier (in the order of 30 kcal mol^{-1}), whereas phenylhydroxycarbene (**2**) gives benzaldehyde (see Scheme 1 on the left).[6,8] In 2011 Mayer et al. investigated the gas-phase reactivity of neutral hydroxymethylene by neutralization–reionization and tandem MS experiments in a three sector field MS instrument.[11] We recently demonstrated in room temperature quadrupole ion trap (QIT) experiments that the charge-tagged phenylhydroxycarbene **3** can be formed and characterized in the gas-phase by collision induced decarboxylation of the corresponding arylglyoxylic acid.[12] In the QIT, in the presence of helium as a buffer gas at millitorr pressure, and at a roughly estimated internal temperature of about 320-350 K, the arylhydroxycarbene **3** rearranges to the charge-tagged aldehyde with a half-life $t_{1/2}$ of about 10 s.[12] With this mechanistic probe in hand, we now present a study of a similar analyte, *i.e.* a charge-tagged phenyl pyruvic acid **4** (Scheme 1 on the right).

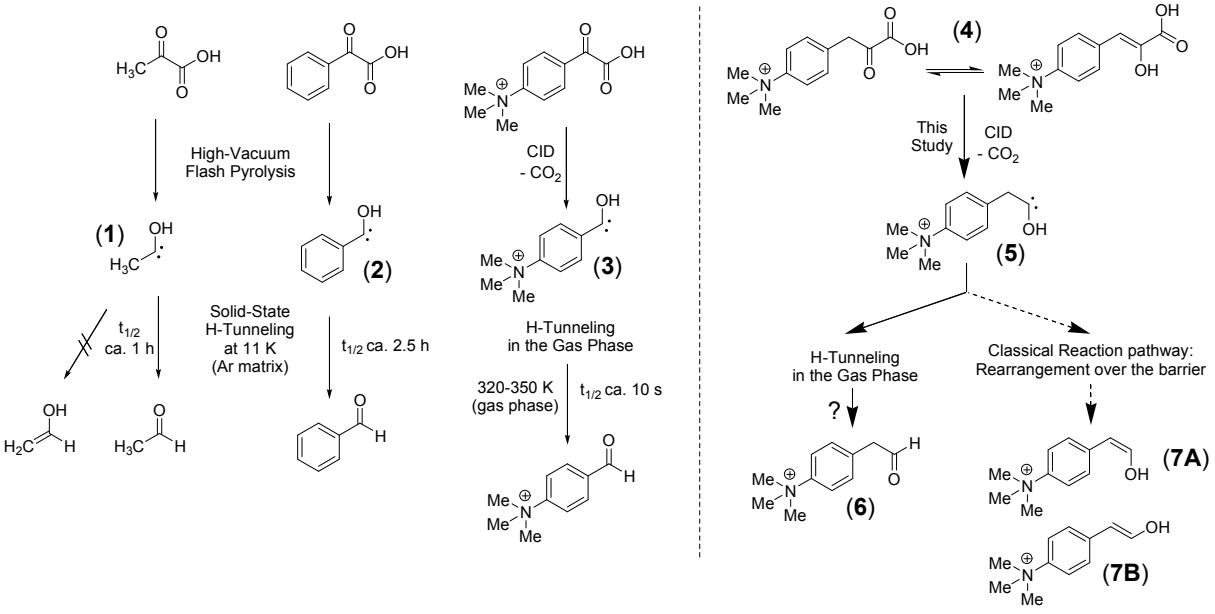

Scheme 1. Left: Quantum-mechanical hydrogen tunneling studied with methylhydroxycarbene (**1**)[6] and phenylhydroxycarbene (**2**)[8] under cryogenic conditions, and above room temperature with the charge-tagged phenylhydroxycarbene (**3**).[12] Right: In this study, the nature and reactivity of CO_2 loss product ions formed by collision induced dissociation (CID) from the charge-tagged phenylpyruvic acid precursor ion **4** are investigated.

2. Results and Discussion

The charge-tagged phenyl pyruvic acid (**4**) was selected to probe whether the charge-tagged benzyl hydroxycarbene **5** is formed via collision induced CO_2 loss in a QIT. Given **5** is formed, we want to investigate the rearrangement reaction to either the aldehyde **6** or the respective enol diastereomer (*Z*: **7A** and *E*: **7B**) tautomers. As in pyruvic acid (the precursor of methylhydroxycarbene (**1**); depicted on the far left), the charge-tagged phenyl pyruvic acid **4** possesses α-methylene protons, which allow tautomerization to enol-acid ion structures (a representative example is included on top of the far right reaction pathway of Scheme 1).[12] As illustrated in Scheme 1, the fixed-charge precursor ions of model compound **4** are transferred into the gas-phase by electrospray ionization (ESI) for analysis in a modified, spherical (3D) QIT mass spectrometer.[13,14] Of foremost interest is to differentiate between the possible ion structures of **4** and also to elucidate the ion structures of the isobaric CO_2 loss tautomer ions (**5**, **6** and **7**) generated by CID in the QIT. Our aim is to collect relevant structural information on the aforementioned analytes by the combination of infrared (IR) ion spectroscopy and theory. For this approach ions of interest are isolated in the QIT and excited with IR photons delivered by an appropriate wavelength tunable light source, e.g. a free electron laser (FEL; wavenumber range 600-1900 cm^{-1}) or an optical parametric oscillator OPO-laser (wavenumber range 3400-3800 cm^{-1}). Whenever the selected ions are on resonance with the laser radiation, non-coherent IR photon absorption and activation occurs, which is regulated by intramolecular vibrational redistribution (IVR). Strong oscillators absorb a sufficient number of IR photons to reach the critical energy barrier of a fragmentation channel and fragment ions are formed and detected in the MS (IR multiphoton dissociation IRMPD).[15-23] IR spectra are acquired by simultaneous monitoring precursor ion depletion and product ion formation as the frequency of the IR radiation is tuned. IR ion spectroscopy is therefore an action spectroscopy method, unlike transmission based IR spectroscopy. The multi photon excitation character in IR ion spectroscopy ultimately determines the typical features of experimental IRMPD spectra such as the observed bandwidths (typically >20 cm^{-1}) and frequency shifts (typically a few %) which get apparent in comparison to linear IR spectra.[24,25] Nevertheless, the assignment of an ion's structure can be confidently obtained when the computed IR spectra of candidate ion structures identified by theory match the recorded data. Many examples document that the identification of individual constitutional isomers, of tautomers, and also of conformers is possible by IR ion spectroscopy.[15-23]

We synthesized the charge-tagged precursor **4** for MS analysis and subsequent tandem-MS generation of the CO_2 loss products. Analogously to our successful investigation of the charge-tagged phenylhydroxycarbene in a QIT,[12] this approach is an attempt to study the quantum-mechanical hydrogen tunneling reactivity of **5** controlling the formation of either the aldehyde **6** *or* the enol diastereomers, *i.e.* the *Z*-enol **7A** and *E*-enol **7B** in the gas phase of a QIT at room temperature (Scheme 1).

2.1 Structure elucidation of the charge-tagged phenyl pyruvic acid 4 in the gas phase

We start with the investigation of the precursor ion structure by (+)ESI-MS and IR ion spectroscopy. The (+)ESI mass spectrum of the charge-tagged phenyl pyruvic acid **4** delivers an abundant molecular ion at *m/z* 222, which is analyzed with IR ion spectroscopy and theory as shown in Figure 1 and 2.

In Figure 1 the computed IR spectra of three enol-carboxylic acid ion structures **4A** – **4C** are compared individually to the recorded gas-phase IR ion spectrum of the charge-tagged phenyl pyruvic acid **4**. Theory predicts the *Z*-enol tautomer **4A** to be the most stable one of all ion structures of **4** in the gas phase (compare ion structures shown in Figure 1 and 2). The linear IR spectrum of **4A** is in good agreement with the measured one in the range of 600-1900 cm^{-1} (see Figure 1A). Ion structure **4A** exhibits strong modes at 1105 cm^{-1} (enol $\nu_{C\text{-}OH}$), 1150 cm^{-1} (COOH $\delta_{O\text{-}H}$), 1310 cm^{-1} (enol $\delta_{O\text{-}H}$); 1400 cm^{-1} (alkene $\delta_{C\text{-}H}$) and, 1730 cm^{-1} ($\nu_{C=O}$).

However, ion structure **4A** has two distinct $\nu_{O\text{-}H}$ stretching modes at around 3430 and 3550 cm^{-1}, which are not found experimentally, making the presence of this ion structure unlikely.

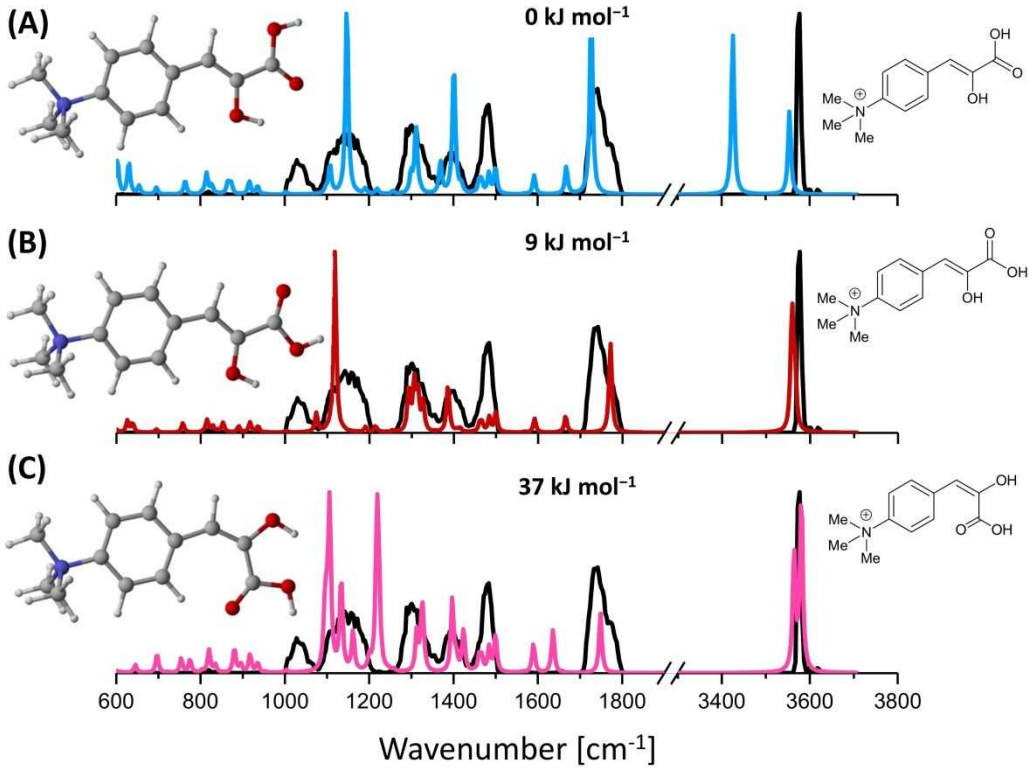

Figure 1. IR ion spectrum of the molecular ion of precursor ion **4** at *m/z* 222 (black trace) compared with the calculated, linear IR spectra of three competitive enol-acid-tautomer ion structures. **(A)** Most stable enol-acid tautomer ion structure **4A** along with the calculated, linear IR spectrum (blue trace). **(B)** IR spectrum of enol-acid tautomer **4B** (red trace). **(C)** IR spectrum of enol-acid tautomer **4C** (pink trace). All band origins of the computed enol-acid-tautomers are presented in Table S5 in the SI. Gibbs energies of compounds given relative to Gibbs energy of enol-acid **4A**.

The IR spectra of other two enol ion structures presented in panels B and C of Figure 1, namely conformers **4B** and **4C** match all features of the measured spectrum (for detailed information on the individual IR modes of ions **4A**-**4C** refer to Table S1 in the SI). In addition, both cations **4B** and **4C** exhibit only one signal referring to the two $\nu_{O\text{-}H}$ vibrations, which overlay at around 3560 cm^{-1}. This agrees well with the experimentally found band. Based on this, we assume that enol-acid tautomer **4B** is mainly present. It is noted that, despite the good spectral agreement of **4C**, the much higher relative energy of that isomer makes its presence less likely. This finding is independently supported by the X-ray crystallographic and ^{1}H-NMR data set of compound **4** and also of the neutral di-methyl-derivative of **4**, which both adopt enol-acid tautomer structures similar to **4A** in the solid state and the condensed phase (see Figures S13 and S20 and also part S4 of the SI for details). The spectroscopic data suggest that enol-acid precursor ion structures are actually formed and that they are energetically favored over keto-acid tautomers. This outcome can be attributed to both the strong electron withdrawing effect of the charge tag in the para position, and hydrogen-bonding interactions which substantially contribute to the stabilization of enol-acid (ion structures **4A** and **4B**) over the alpha-keto acid tautomer ion structures (**4D** and **4E**, see Figure 2). Finally, we note that the band at around 1028 cm^{-1} in the recorded spectrum of **4** shown Figure 1 finds no counterpart in the IR spectra of the ion structures **4A**-**4C**, suggesting that an additional ion structure is contributing.

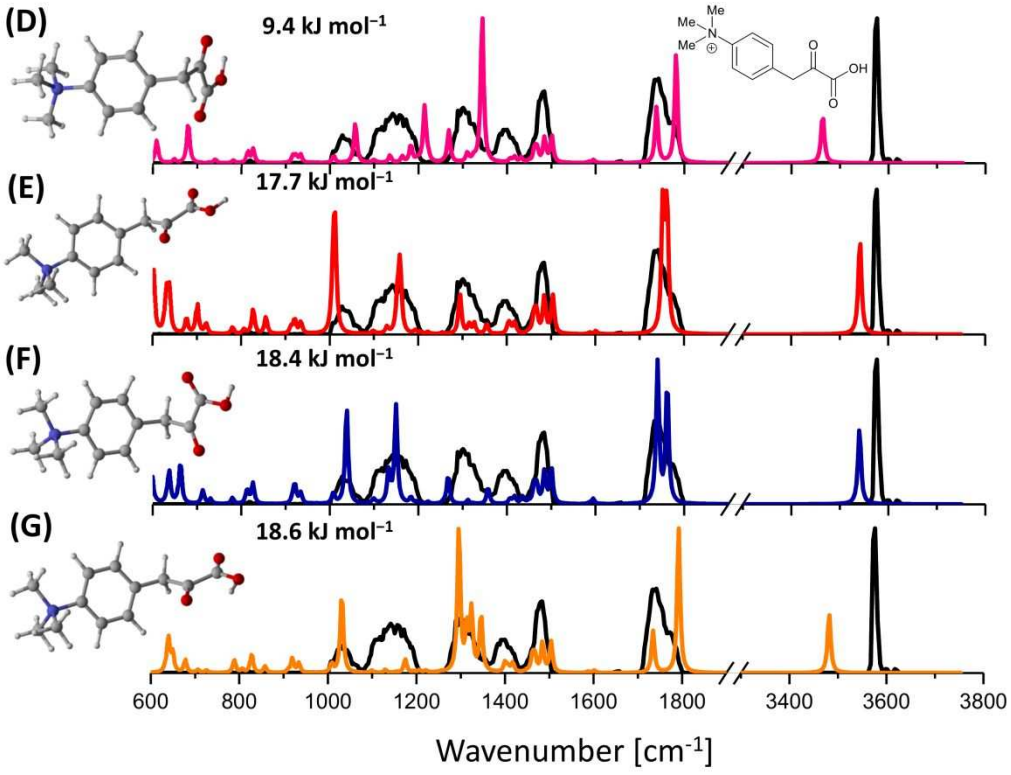

Figure 2. IR ion spectrum of the molecular ion of precursor ion **4** at *m/z* 222 (black trace) compared with the calculated, linear IR spectra of four competitive α-keto-acid conformers. **(D)** IR spectrum of α-keto-acid **4D** (pink trace). **(E)** IR spectrum of α-keto-acid **4E** (red trace). **(F)** IR spectrum of α-keto-acid **4F** (blue trace). **(G)** IR spectrum of α-keto-acid **4G** (orange trace). All band origins of the computed keto-tautomer ion structures are presented in Table S6 in the SI. Gibbs energies of compounds given relative to Gibbs energy of **4A**.

In Figure 2 four computed α-keto-carboxylic acid ion structures **4D** – **4G** are presented along with their linear IR spectra in comparison to the recorded gas-phase IR ion spectrum of the charge-tagged phenyl pyruvic acid **4**. The computed IR ion spectra of conformers **4E** and **4F** are in good overall agreement with the experimental IR ion spectrum of precursor ion **4**. Both ion structures **4E** and **4F** even provide an absorption band matching the signal at 1028 cm^{-1} ($\nu_{carbonylC\text{-}CH2}$, see Table S6 in the SI), suggesting their presence along with candidate structure **4B**. However, theory suggests that both **4E** and **4F** are considerably less stable than the best match, i.e. the enol-acid ion structure **4B**. The other two conformers **4D** and **4G** shown in Figure 2 can be excluded on the basis of their red shifted $\nu_{O\text{-}H}$ vibrations, compared to the experimental signal.

The finding that the enol-acid ion structure **4B** is most likely present in the gas phase, despite the fact that it is not the gas-phase ground state ion structure, *i.e.* **4A**, prompted us to perform additional calculations to probe whether the identified ion structures are remnants of lower-energy solution-phase structures. Carry-over effects of solution-phase favored ion structures into the gas phase, which are there kinetically trapped after the electrospray process, have been observed and reported numerous times.[26-28] In a previous study on the thione-thiol tautomeric equilibrium of ergothionein (2-mercaptohistidine trimethylbetaine, ET), we found clear evidence that cationic molecular ions of ET conserve their condensed-phase ground state, *i.e.* a thione ion structure in the gas phase.[29] To probe this aspect, a number of geometry optimizations were performed using a simulated MeOH solvent environment. In particular, we investigated isomers **4B**, **4C**, **4E**, and **4F** as the most probable isomers in the gas phase, based on the experimental IRMPD data. In addition, **4A** was included as well,

since it is calculated to be the lowest-energy isomer in the gas phase. The MeOH solvent environment was simulated using polarizable continuum model PCM[30,31] with three added MeOH molecules to partially simulate the first solvation shell. The resulting structures, labelled **4A'**, **4B'**, **4C'**, **4E'**, and **4F'** are depicted in Figure 3 in order of their free energies relative to the lowest energy isomer, **4B'**. Two conclusions can be drawn from Figure 3. First of all, the energetic ordering for the enol-acid isomers changes from the solution phase to the gas phase. In the solution phase **4B'** is the lowest-energy isomer, followed by **4A'**, whereas in the gas phase **4A** is lower in energy than **4B**. **4C'** and its gas phase complement **4C** are the least stable isomers for this motif. Secondly, the keto-acid structures are still less stable with free energies more than 3.8 kJ mol^{-1} above **4B'**. Thus, whilst the difference is smaller, our calculations provide evidence that the enol form **4B** is the likely tautomer in the gas phase and that the most favoured solvation-phase structure is maintained upon evaporation.

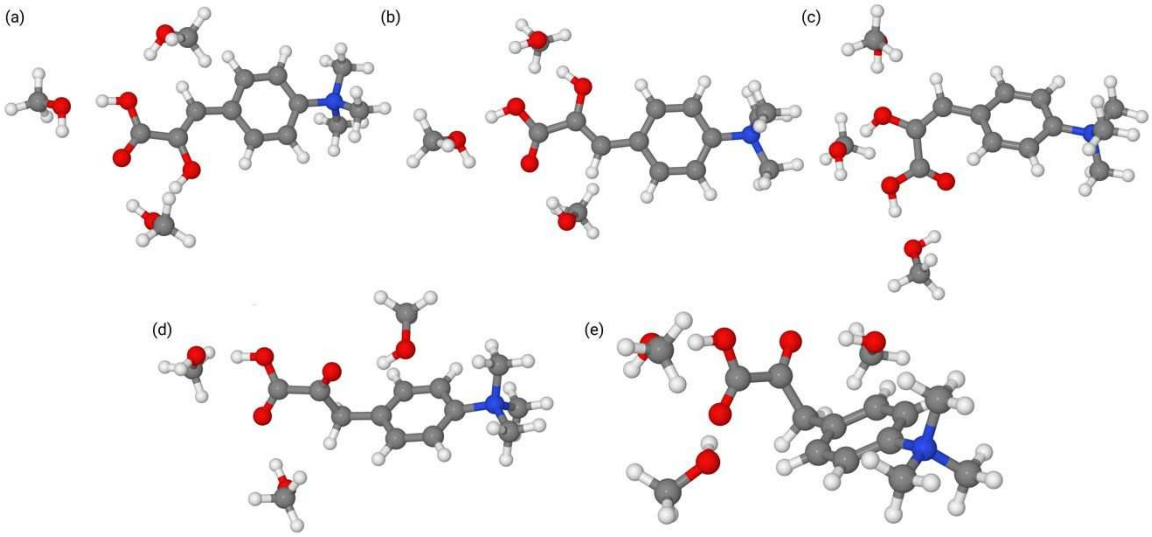

Figure 3. Simulated solvation phase structures with 3 methanol molecules, which mimic the first solvation shell with free energy differences with respect to **4B'** indicated. Panel (a): **4B'** (0.0 kJ mol^{-1}). Panel (b): **4A'** (2.9 kJ mol^{-1}). Panel (c): **4C'** (30.6 kJ mol^{-1}). Panel e: **4E'** (3.8 kJ mol^{-1}). Panel (e): **4F'** (6.1 kJ mol^{-1}).

In conclusion, we find IR ion spectroscopic evidence for the predominant formation of an enol-acid precursor ion structure, namely ion structure **4B**. This is not the most stable structure suggested by theory in the gas phase, but it is the most stable structure in the solution phase. The computational outcome, favoring an enol-acid tautomer (**4B'**) can be related to the beneficial hydrogen bonding network established in the enol-acid moiety. Additionally, the strong electron-withdrawing influence of the positively charged para-tri-methyl-ammonium substituted phenyl ring further contributes to the stabilization of the enol-acid over the α-keto-acid tautomers **4D** – **4G** vs. **4B**.[32] Aside from this, we analyzed the ion structure of the triply deuterated precursor ion $\mathbf{4_{3D}}$ resulting from solution phase H/D exchange and observed identical results confirming our assumption for precursor **4** (see parts S1.2 and S2.2 in the SI).

2.2 Structure elucidation of the CID product ions of precursor 4

As discussed above and illustrated in Scheme 1, we synthesized the charge-tagged phenyl pyruvic acid **4** to study the gas-phase reactivity of the benzyl hydroxycarbene **5**. The QIT-MS^2 product ion spectrum of the molecular ion of precursor **4** at *m/z* 222 shows a prominent

loss of 44 Da, *i.e.* the loss of CO_2 (the ESI-MS^2 spectrum is presented in Figure S1 in the SI). The product ion at *m/z* 178 was then subjected to IR spectroscopic analysis and an IR ion spectrum was recorded by simultaneous monitoring precursor ion depletion and the formation of the photo fragment ions at *m/z* 162 (loss of CH_4) and *m/z* 133 (loss of $(CH_3)_2NH$) as the photon energy was tuned. This IR ion spectrum of the ion at *m/z* 178 is then compared to the ones of candidate ion structures proposed by theory, see Figures 4, 5, and 6.

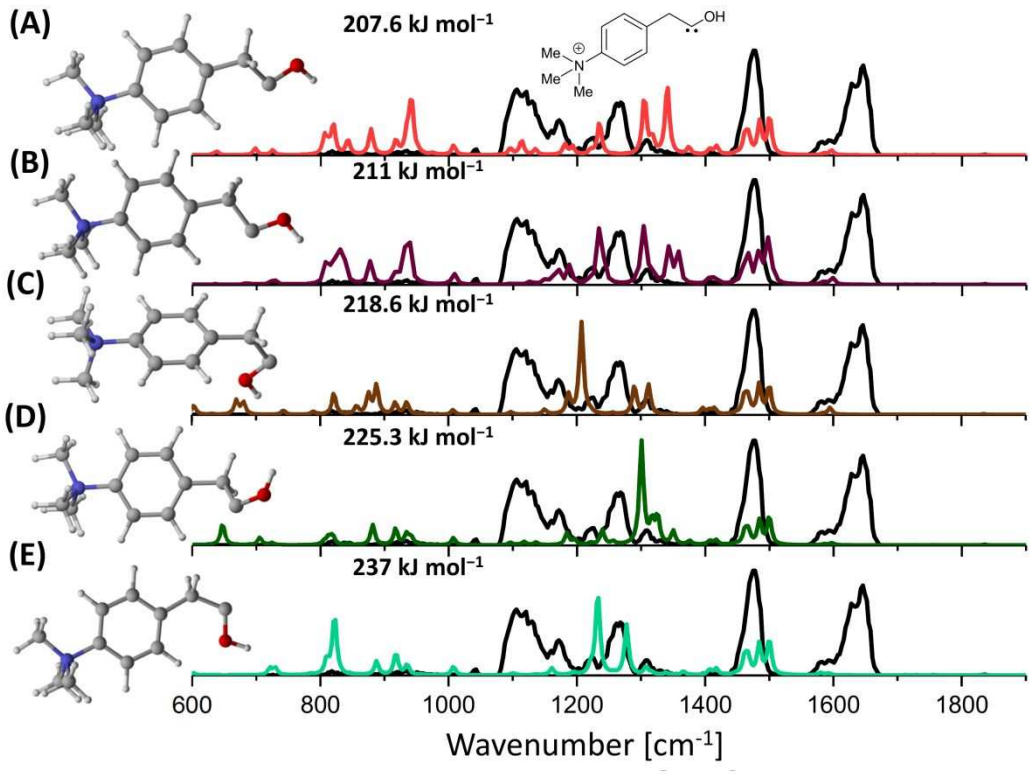

Figure 4. IR ion spectrum of the CID product ion formed by CO_2 loss from precursor **4** at *m/z* 178 (black trace) compared to the IR ion spectra of five charge-tagged benzyl hydroxycarbene ion structures along with the calculated, linear IR spectra. **(A)** Single bond trans hydroxycarbene ion structure **5A** (red trace). **(B)** Hydroxycarbene conformer **5B** (blue trace). **(C)** Single bond cis hydroxycarbene conformer **5C** (brown trace). **(D)** Single bond trans hydroxycarbene **5D** (pink trace). **(E)** Single bond cis hydroxycarbene conformer **5E** (green trace). All band origins of the computed hydroxycarbene ion structures are presented in Table S9 in the SI. Gibbs energies of compounds given relative to Gibbs energy of aldehyde **6**.

In Figure 4 the acquired IR ion spectrum of the CO_2 loss product ion at *m/z* 178 is compared to the computed ones of a series of hydroxycarbene ion structures identified by theory. All hydroxycarbene ion structures **5A** – **5E** are energetically highly unfavored compared to the most stable ion structure, *i.e.* the aldehyde **6**, depicted in Figure 5. The different conformers of **5** fall into two broad groups. In the first group (**5A**, **5B**, and **5D**), the main interaction between the phenyl ring and the hydroxycarbene moiety is a van der Waals interaction between the *ortho* hydrogen atom on the phenyl ring and the lone pair on the carbon atom of the hydroxycarbene. In the second group that interaction is between the oxygen atom of the hydroxycarbene. In the second group (**5C** and **5E**) that interaction is between the oxygen atom of the hydroxycarbene and the *ortho* hydrogen atom on the phenyl ring. Inspection of the recorded IR ion spectrum in comparison with the computed ones clearly indicates that the benzyl hydroxycarbenes **5A** – **5E** cannot solely be responsible for the experimental results as at least two strong bands are not accounted for (bands at 1100 – 1150 cm^{-1} and

1600 – 1670 cm^{-1}). However, the broad band at around 1480 cm^{-1} found in the measured data set (black trace in Figure 4) could be a composite signal of the set of three modes found in all computed IR spectra of the hydroxycarbene ion structures. In the aforesaid range of 1450–1500 cm^{-1} all hydroxycarbenes perform methyl C-H stretching and bending as well as aromatic in plane bending modes. However, **5C** and **5E** have strong absorptions around 1200 cm^{-1}, where experimentally no strong absorptions are found.

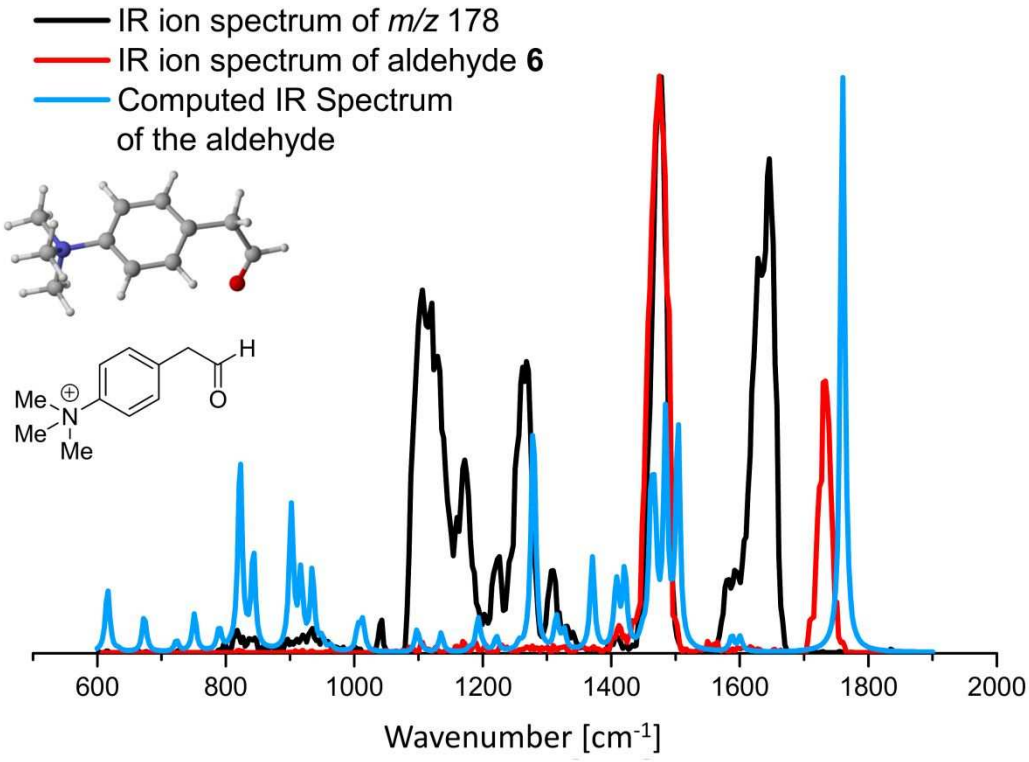

Figure 5. IR ion spectrum of the CID product ion formed by CO_2 loss from precursor **4** at *m/z* 178 (black trace) compared with the IR ion spectrum of reference aldehyde **6** (red trace) compared with the calculated, linear IR spectrum of aldehyde ion structure identified by theory as depicted in the inset (blue trace). All band origins of the computed aldehyde ion structure **6** are presented in Table S8 in the SI.

In Figure 5 we compare the computed IR spectrum of the ion structure of the aldehyde proposed by theory (ion structure included in Figure 5; blue trace) with the IR ion spectrum of the molecular ion of the aldehyde reference compound **6** at *m/z* 178 (red trace; see parts S1.3 and S2.3 in the SI for details) and the IR ion spectrum of the CO_2 loss product, generated by CID of precursor **4** (black trace). The strong carbonyl stretching mode $\nu_{C=O}$ at around 1750 cm^{-1} is missing in the IR ion spectrum of the CID product ion (black trace in Figure 5). This clearly indicates that aldehyde **6**, the expected product of [1,2]H-shift rearrangement potentially formed via quantum-mechanical hydrogen tunneling of the hydroxycarbene ion structures **5A** – **5E** is not formed at all by CO_2 loss from **4**.[6] This decisive finding sets the gas-phase behavior of precursor **4** and that of its decarboxylation product ion clearly apart from that of the phenyl analogue and its decarboxylation product ion, hydroxycarbene **3**, which exclusively delivers benzaldehyde (compare Scheme 1).[12]

Finally, we have examined the enol tautomers identified by theory on the basis of the IR spectra. Figure 6 presents an overview of IR ion spectra of the three relevant enol ion structures **7A** – **7C**. Our DFT calculations suggest that the *Z*-enol ion structure **7A** is more stable than the *E*-diastereomer enol **7B** (by 5 $kJmol^{-1}$). This is caused by a van der Waals

interaction between the enol oxygen and the adjacent *ortho* hydrogen attached to the electron poor phenyl ring as depicted in Figure 6. The IR spectra of the enol tautomers are in good agreement with the recorded spectrum of the ion at *m/z* 178 formed by CO_2 loss from precursor **4**. Inspection of Figure 6 implies that an overlay of the computed IR spectra of enols **7A** and **7B** could explain all bands found, indicating the simultaneous presence of at least these two enol stereoisomers. Similar to the hydroxycarbenes the strong absorption at around 1480 cm^{-1} could also result from the three minor bands found in the computed spectra of **7A** and **7B** in this wavenumber range. The enol tautomers perform analogous vibrations in the aforesaid range of 1450 – 1500 cm^{-1}, i.e. methyl C-H stretching and bending as well as aromatic in plane bending modes. The fact that the two enol diastereomers **7A** and **7B** are energetically in a similar range further supports the identification and makes their concomitant presence possible. Additionally, we analyzed the ion structure of the CO_2 loss product at *m/z* 181 generated from the triply deuterated precursor ion $\mathbf{4_{3D}}$ using IR ion spectroscopy. Consistent with our results discussed above, we identify the respective enol ion structure $\mathbf{7A_{3D}}$ and find also no evidence for the formation of the aldehyde $\mathbf{6_{3D}}$ (see part S2.5 in the SI).

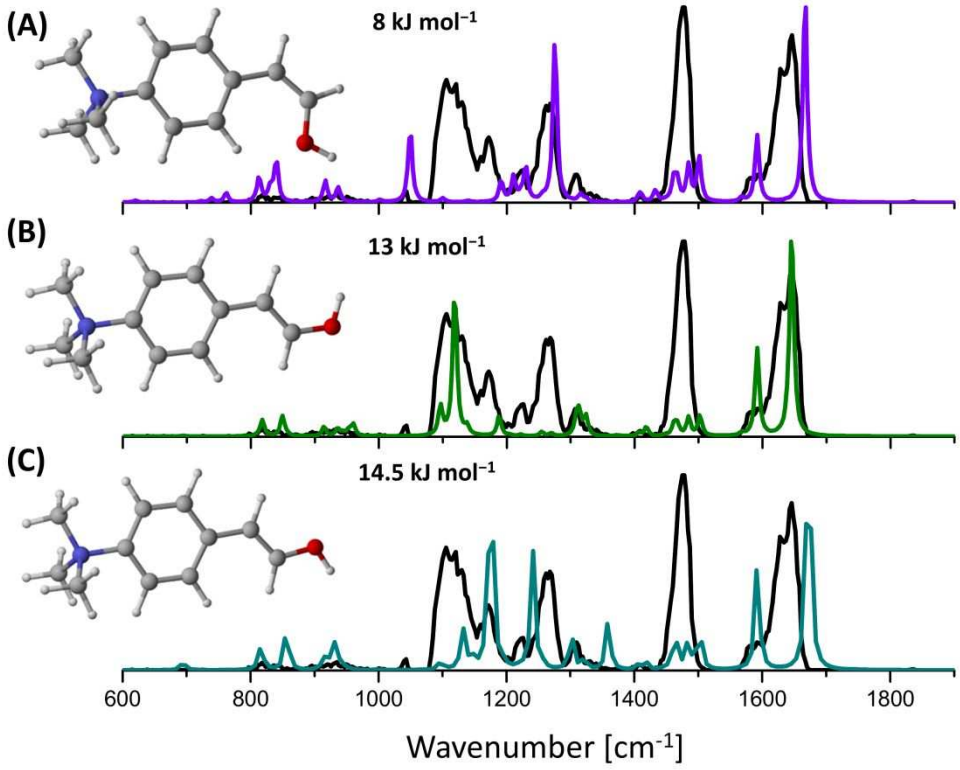

Figure 6. IR ion spectrum of the CID product ion formed by CO_2 loss from precursor **4** at *m/z* 178 (black trace) compared to the IR ion spectra of three competitive enol ion structures along with the calculated, linear IR spectra. **(A)** Ion structure of *Z*-enol **7A** (purple trace). **(B)** Ion structure of *E*-enol **7B** (green trace). **(C)** A second *E*-enol **7C** conformer (pink trace). All band origins of the computed enol ion structures are presented in Table S10 in the SI. Gibbs energies given relative to the Gibbs energy of the aldehyde **6**

Thus, theory and spectroscopy are indicating the formation of enol diastereomers **7A** and **7B** upon CO_2 loss as discussed above and illustrated in Scheme 1. However, we note that the IR ion spectrum of the decarboxylation product ion is not completely unambiguous, since it does not exhibit any *unique* spectral signature allowing an assured identification of any of the benzyl hydroxycarbenes **5A** – **5E**, nor can a complete exclusion of the hydroxycarbenes be justified. It is clear, though that the aldehyde **6** is not formed. These results suggest that

either the formation of the energetically very much unfavored hydroxycarbenes is avoided or that if hydroxycarbenes are intermediately generated, they tautomerize rapidly and exclusively to the enol(s) rather than to the aldehyde. To scrutinize the reaction mechanism of the CO_2 loss process starting from the enol-acid precursor ions identified to enol-product ion structures in more detail, we performed dedicated DFT calculations, which are discussed in the next part.

2.3 Computational analysis of the reaction pathway from the enol-acid precursor to the enol product ions in gas-phase CID experiments

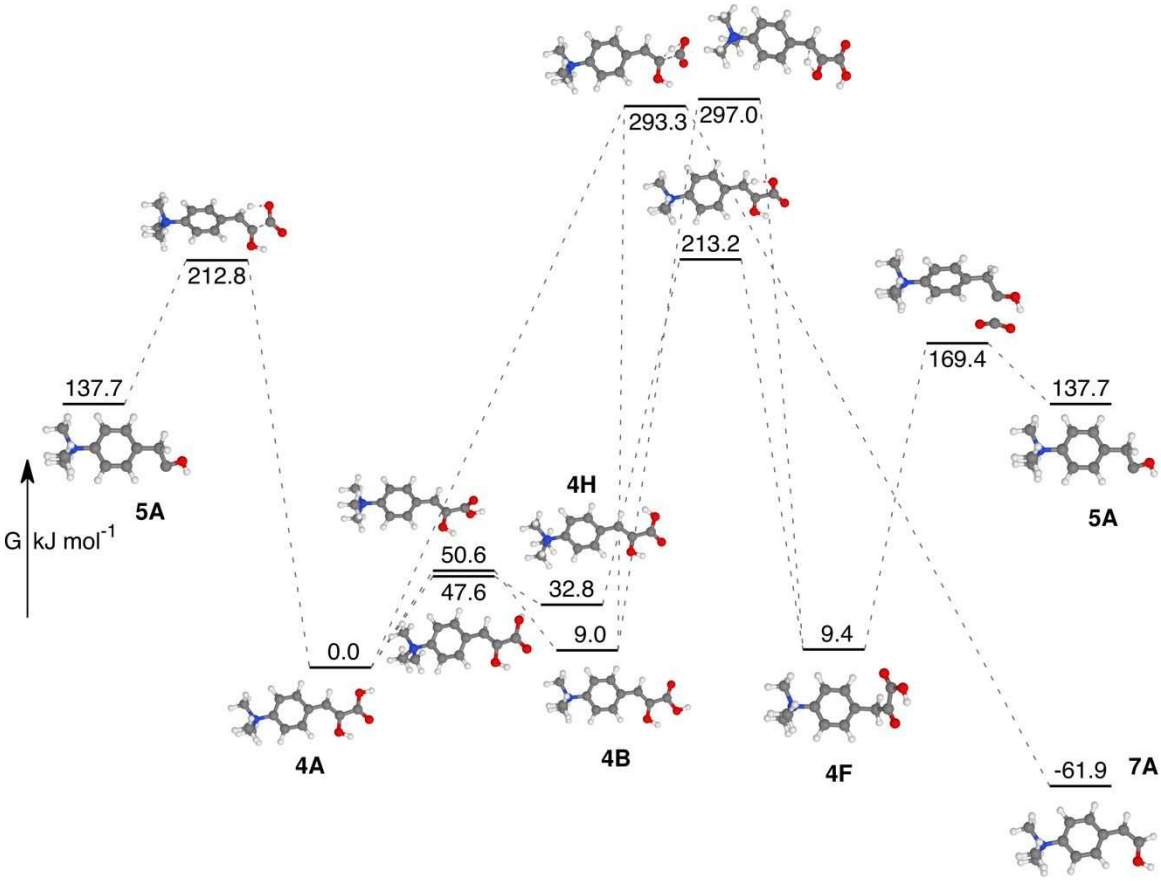

Figure 7. Computational analysis of potential rearrangement reactions and decarboxylation processes upon collisional activation in a MS^2 experiment (ΔG_{298K}). The enol-acid precursors **4A** and **4B** deliver *Z*-enol tautomer **7A** via the same transition state at 293.3 kJ mol^{-1}. Precursor ions **4A** as well as **4F** reach hydroxycarbene **5A** directly. The tautomerization reaction from **4B** to **4F** can be accomplished via a 2 proton shift (TS at 213.2 $kJmol^{-1}$) or via an energetically more demanding 1 proton shift (TS at 297.0 kJ mol^{-1}).

Previously, we carefully studied the decarboxylation reaction of oxo[4-(trimethyl-ammonio)-phenyl]acetic acid and the reactivity of the respective phenylhydroxycarbene **3**.[12] Extensive DFT calculations provided a clear rationalization of the gas-phase dissociation pathways of the tailor-made precursor as well as of the subsequent decay of its CID products via quantum mechanical hydrogen tunnelling. Here, we analyse the rearrangement and dissociation behaviour of a charge-tagged phenyl pyruvic acid derivative, wherefore multiple reaction pathways of a set of precursor ion structures have to be considered and evaluated. In Figure 7 the modeled reaction network starting from the gas-phase ground state enol-acid ion structure **4A** is depicted. From there pathways lead to specific product ion tautomer structures, such as the hydroxycarbene **5A**, the aldehyde **6**, and the enol ion structure **7A**.

First, we probe the isomerization of the precursor ion structures upon collisional heating prior to dissociation.[31] This route starts from the most likely isomer found in the gas-phase, *i.e.* the enol-acid ion structure **4B** (compare Figure 1 and 3), leads to conformer **4A**, and ultimately to the hydroxycarbene **5A**. According to our calculations, the transformation from enol acid **4B** into conformer enol acid **4A** is relatively facile with a barrier of 50.6 kJ mol^{-1}. The subsequent loss of CO_2 to form **5A** has a barrier of 212.8 kJ mol^{-1}. Here, we note that this is significantly higher than the free energy barrier of 136.3 kJ mol^{-1} found in reference 11.

From enol acid **4B** there is also an alternative pathway leading to keto acid **4F** through an initial enol-keto isomerisation. It is well known that isolated enols are kinetically trapped in the gas phase by a high energy barrier rendering enol-keto tautomerization without any acid or base catalysis very slow.[31] Indeed, our calculations show that a standard [1,2]-hydrogen-shift from the hydroxyl group to the α-carbon to generate the ketone has a free energy barrier of 297.0 kJ mol^{-1}. This is clearly unfeasible, particularly in relation to the more facile transformation of **4B** into **4A** onto hydroxycarbene **5A**. However, our calculations also suggest that there is second pathway from enol acid **4B** via **4A** to keto acid **4F**. This involves an OH rotation to reach **4H** followed by a 2-hydrogen shift with one hydrogen moving from the acid group onto the α-carbon. This is then followed by the second hydrogen moving from the hydroxyl group to the adjacent carbonyl oxygen. This process has a free energy barrier of 213.2 kJ mol^{-1}, which makes it competitive with the **4B** to **4A** to hydroxycarbene **5A** route. In a subsequent decarboxylation reaction pathway, the keto acid **4F** reaches hydroxycarbene **5A** via a transition state at 169.4 kJ mol^{-1}, which is in the range of the barrier found for the formation of **3** (136.3 kJ mol^{-1}).[12]

Our IR spectroscopy results clearly showed evidence for the presence of the enol-acid precursor **4B** and the enol product ion tautomer **7A** and/or **7B** in the gas phase (see Figures 1 and 5). Therefore, DFT calculations were performed to investigate the direct formation of **7A** or **7B** from **4A** or **4B** as well as from **5A**. Two relevant reaction pathways were identified by theory in this respect. Direct decarboxylation of the enol acid **4B** (as well as from **4A**) can directly lead to the *Z*-enol product ion structure **7A**. However, this has a free energy barrier of 293.3 kJ mol^{-1}, making it uncompetitive with respect to the transformation of **4B** into **5A** via either of the two pathways defined above. On the basis of these computational results, we have to assume that hydroxycarbene **5A** might be formed as a primary and short-lived reaction intermediate of the CID degradation of enol-acid precursor ion **4B** in the multiple collision activation process experiment.[33] Thus, consideration needs to be given to the decay pathways of **5A**. Hereby, it should be noted that it cannot lead to formation of the aldehyde **6**, since this tautomer was not detected spectroscopically. These pathways are depicted in Figure 8. For the hydroxycarbene **5A**, there are two competing [1,2]H-shift reaction channels. Due to the presence of the neighbouring methylene moiety, **5A** can either rearrange to the aldehyde **6** over a free energy barrier of 130.5 kJ mol^{-1}, or to the *E*-enol **7C** over a free energy barrier of 88.2 kJ mol^{-1}. Once **7C** is reached, there is only a small barrier to **7B**, which should therefore be experimentally accessible. The energetic profile of hydroxycarbene **5A** shown in Figure 8 is therefore qualitatively similar to the one governing the reactivity of the neutral methylhydroxycarbene (see **1** in Scheme 1).[6,10] However, quantitatively there is one significant difference to methylhydroxycarbene.[6] In our case, the barrier to the formation of the aldehyde **6** is higher, whereas the barrier to formation of the enol **7C** is lower than the equivalent transformation in ref 6. In particular, Schreiner et al. report transition enthalpies of 117.0 kJ mol^{-1} and 94.6 kJ mol^{-1}, respectively.[6] In our current study the equivalent *enthalpies* are 132.4 kJ mol^{-1} and 84.6 kJ mol^{-1}, respectively. In our previous study, we calculated a transition enthalpy for the isomerisation of carbene **3** to the corresponding aldehyde of 128.1 kJ mol^{-1},[12] which is also lower than for the current study.

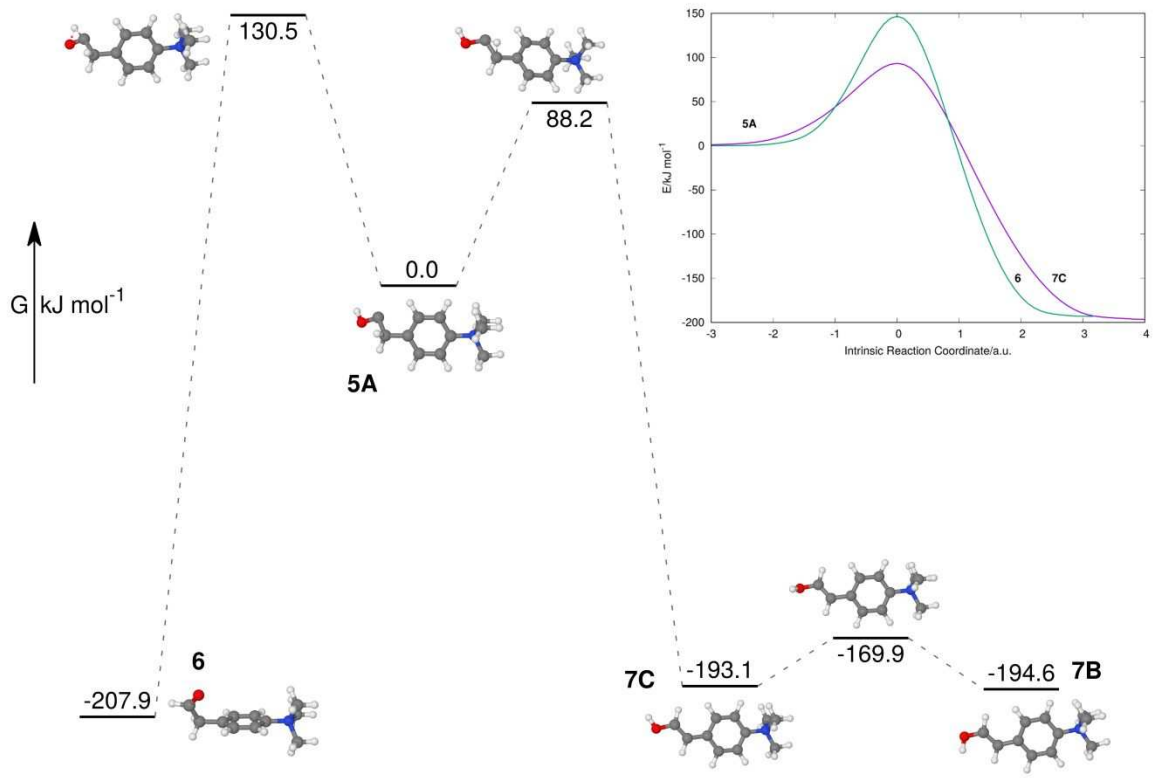

Figure 8. Computational analysis of the decay mechanism starting from the hydroxycarbene **5A** to either the enols **7C** and **7B** and the aldehyde tautomer **6** (ΔG_{298K}). Intrinsic reaction coordinate (IRC) profile for the conversion of hydroxycarbene **5A** into aldehyde **6** and enol **7C**. The IRCs have been computed using dispersion-corrected DFT using the B3LYP-GD3BJ functional and the cc-pVTZ basis set with frequencies calculated at every step of the IRC process.

In this regard it is important to note, that Schreiner *et al.* investigated the methylhydroxycarbene **1** at cryogenic temperatures of 11K in a solid argon matrix and found that it cleanly penetrates the more narrow (but higher) energy barrier leading to the exclusive formation of acetaldehyde via quantum mechanical hydrogen tunneling.[6] Our setup is, of course, very different from the experimental setup used for matrix spectroscopy. We investigate product ions generated upon multiple collision dissociation processes. The hot ions are immediately thermalized in the linear quadrupole ion trap leading to internal ion temperatures of at least 300 K by virtue of the dissipative collisions with the helium buffer gas present at millitorr pressures.[12] The fundamental finding, that aldehyde **6** is not observed at all (compare Figure 5) means that the pathway to an enol is the exclusive degradation pathway of hydroxycarbene **5A** as Figure 8 illustrates. Our experimental results with D_3 isotopologues yield identical results. Thus, we do not find any indication for isotopic discrimination (see parts S2.2 and S2.5 in the SI). Hence, we assume that the lower barrier towards formation of the enol (suggesting a 55-fold increase in the over-the-top rate, if a simple Arrhenius rate is assumed), and a substantially higher barrier to the aldehyde **6**, leads to an exclusive decay of hydroxycarbene **5A** to ultimately enol **7B**. Given the higher dissociation energy for **4** compared to the system studied before, we would expect **5A** to be formed initially more excited than the equivalent hydroxycarbene **3**.[12] This should actually enhance tunnelling towards the aldehyde **6**, since the barrier is narrower towards the top of the barrier. As aldehyde **6** is not identified spectroscopically, we instead conclude that all hydroxycarbene ions **5A** are converted into **7B** via **7C**.

In summary, the results suggest that hydroxycarbene **5A** can overcome the respective barrier to form enol **7B** via the transition state at 88.2 kJ mol^{-1} depicted in Figure 8, but **5A** is

blocked energetically from reaching aldehyde **6**. Consequently, the internal energy of the transient hydroxycarbene **5A** species should lie right over the TS of the enol pathway but significantly below the energy demand of the aldehyde route. Since aldehyde **6** is not generated at all (the respective barrier width is smaller than that of the barrier towards the enol; Figure 8), we conclude that hydrogen tunnelling is not contributing under the given experimental conditions.

Conclusions

We have analyzed a charge-tagged phenyl pyruvic acid derivative by tandem-MS in a 3D QIT, IR ion spectroscopy and theory. The effective CO_2 loss by CID allows access to investigate the structure and the reactivity of the product ions formed. The IR ion spectrum of the precursor ion points towards the formation of an enol-acid rather than an α-keto acid tautomer ion structure in the gas phase before the collisional activation events. Furthermore, it is clear from the IR spectra that at least predominantly – if not exclusively – enol tautomers are formed by CO_2 loss. However, a transient formation of hydroxycarbenes, suggested by our DFT computations, cannot be proven or ruled out experimentally. The potential energy surface established for the hydroxycarbene products, implicates that the enol ions, clearly identified by IR ion spectroscopy, can be formed in a secondary rearrangement process. In contrast to that, quantum mechanical tunneling of the hydroxycarbenes can be excluded, since no evidence for aldehyde product ion formation is observed. This outcome is attributed to the initially highly excited energy levels of the product ions formed by CID, which allow access over the energy barrier for rearrangement leading to the ultimate formation of the enol-tautomer ions identified by IR ion spectroscopy. This study therefore highlights the impact of the experimental settings and preconditions on the outcome, since methylhydroxy-carbene stored at cryogenic temperatures in an argon matrix cleanly penetrates the substantial energy barrier to form exclusively acetaldehyde via quantum mechanical hydrogen tunneling.[6]

3. Experimental

3.1. Materials

Compound **4** was synthesized for this study as discussed in the Supporting information (see Supporting Information part S3 for details).

3.2 Mass Spectrometry

Compound **4** was dissolved (c ~ 10^{-5} M) in CH_3OH for (+)ESI-MS and MS^2 experiments. All (+)ESI, tandem-MS and accurate ion mass measurements were conducted on an LTQ-Orbitrap XL instrument (ThermoFisher, Bremen Germany). Accurate ion mass measure-ments were executed in the orbitrap analyzer with a resolution of 30000 fwhm with external calibration (Δm < 3 ppm) or with addition of internal standards (Δm < 2 ppm) by a lock mass procedure. The product ion experiment of **4** was performed in the linear ion trap (LTQ) part of the LTQ-Orbitrap XL instrument by CID with the He bath gas present (P = 2 × 10^{-5} Torr; 2.7 mbar). The product ions were analyzed in the orbitrap (see Figure S1 in the Supplementary Information). Typical (+)ESI-MS conditions: Flow rate: 5 µL min^{-1}; Capillary voltage: 3.20 kV; Sheath gas: 4.99 [arb. units]; Aux gas: 2.00 [arb. units]; resolution: 30000 fwhm. Additional MS-data and spectra are presented in the SI in part S1.

3.3. Infrared Ion Spectroscopy

A modified 3D quadrupole ion trap mass spectrometer (Bruker, Amazon Speed) was used for the infrared (IR) ion spectroscopy study, which has been described in detail elsewhere.[13] The 3D quadrupole ion trap was operated at ambient temperature (~320 K) with He buffer gas at a pressure of ~10^{-3} mbar.[13] Wavelength tunable laser radiation was generated by the Free Electron Laser for Infrared eXperiments (FELIX)[13,14,35] in the 600−1900 cm^{-1} range for all photo dissociation experiments. Additionally, a pulsed OPO (LaserVision, USA) source was

used to cover the 2800−3700 cm^{-1} range. Both lasers operate with a repetition frequency of 10 Hz. The FEL pulse energies were approximately 50-100 mJ per 5 μs long macropulse and OPO delivered 10−20 mJ per 5 ns long pulse. The full width at half-maximum bandwidth of the FEL is approximately 0.4% of the central wavelength and 3 cm^{-1} for the OPO. Gas-phase precursor ions for IR ion spectroscopy were generated by electrospray ionization in positive ion mode from solutions of 0.5 μM in methanol at a flow rate of 120 μL h^{-1}. Ions were irradiated for 1 s, corresponding to interaction with 10 laser pulses. The IR spectra result from a series of mass spectra recorded while the FEL was scanned over the wavenumber range from 600−9cm^{-1}. The depletion of the precursor ion signal as well as the increase of intensity of the photo dissociation product ion peaks are monitored as a function of IR frequency. Unimolecular dissociation results from the absorption of multiple IR photons (IRMPD) with effective intramolecular vibrational redistribution of the excitation energy leading to non-coherent photo activation until the threshold for dissociation is reached.[15-23] The IR yield ($\Sigma I_{fragment\ ions}/\Sigma I_{all\ ions}$) was determined after laser irradiation at each frequency and was linearly corrected for frequency-dependent variations in laser power. A grating spectrometer (wavemeter) was used to calibrate the absolute frequency of the FEL (OPO).

3.4 Computations

Density functional theory (DFT) calculations were performed using Gaussian09, version D.01.[34] Gaussian was compiled with Gaussian-supplied versions of BLAS and ATLAS.[35,36] The B3LYP functional was used throughout with the GD3-BJ correction to account for dispersion interactions, whereby it is noted that in this case this correction did not change results significantly compared to the bare B3LYP functional.[39,40] The cc-pVTZ basis set was used throughout with the ultrafine setting for the integrals.[41,42] This computational procedure was found to give good correlation with experiment in previous work.[12] All the calculations performed on these systems were done in vacuo. Frequencies were scaled by 0.97 in the wavenumber range of 600-1900 cm^{-1} and in the wavenumber range of 3400-3800 cm^{-1} with a factor of 0.95 to account for anharmonicity and convoluted with a Gaussian line shape function with a FWHM of 12 cm^{-1} to facilitate comparison with experiment.[29,31,43] Energy differences quoted throughout the paper are based on Gibbs free energies (298 K, 1 bar). All transition states were checked to connect the correct energy minima through an intrinsic reaction coordinate calculation.[44,45]

Conflicts of interest

There are no conflicts to declare.

Acknowledgements

The authors thank the entire FELIX staff for skillful assistance. Funding from LASERLAB-EUROPE (grant agreement no. 654148, European Union's Horizon 2020 research and innovation program), and by the Deutsche Forschungsgemeinschaft (DFG) grant numbers SCHA 871/10-1 and BE 998/16-1 is gratefully acknowledged.

Appendix A. Supplementary data

Supplementary data associated with this article can be found, inthe online version, at

Keywords
IR Ion Spectroscopy | Density Functional Theory Computations | Hydroxycarbene Formation |

References

1 S. Diez-Gonzales (ed.) N-Heterocyclic Carbenes: From Laboratory Curiosities to Efficient Synthetic Tools, 2nd Ed., RSC Catalysis Series No 27, The Royal Society of Chemistry, Cambridge, UK, 2017.
2 M. N. Hopkinson, C. Richter, M. Schedler, F. Glorius, *Nature* 2014, **510**, 486.
3 D. Enders, O. Niemeier, A. Henseler, *Chem. Rev.* 2007, **107**, 5606.
4 A. Berkessel, S. Elfert, V. Reddy Yatham, J-M. Neudörfl, N. E. Schlörer, J. H. Teles, *Angew. Chem. Int. Ed.* 2012, **51**, 12370.
5 A. Berkessel, V. Reddy Yatham, S. Elfert, and J-M. Neudörfl, *Angew. Chem. Int. Ed.* 2013, **52**, 11158.
6 P. R. Schreiner, H. P. Reisenauer, D. Ley, D. Gerbig, C.-H. Wu, W. D. Allen, *Science* 2011, **332**, 1300.
7 P. R. Schreiner, H. P. Reisenauer, F. C. Pickard IV, A. C. Simmonett, W. D. Allen, E. Mátyus, A. G. Császár, *Nature* 2008, **453**, 906.
8 D. Gerbig, H. P. Reisenauer, C.-H. Wu, D. Ley, W. D. Allen, P. R. Schreiner, *J. Am. Chem. Soc.* 2010, **132**, 7273.
9 P. R. Schreiner, *J. Am. Chem. Soc.* 2017, **139**, 15276.
10 D. Ley, D. Gerbig, J. P. Wagner, H. P. Reisenauer, P. R. Schreiner, *J. Am. Chem. Soc.* 2011, **133**, 13614.
11 Y. Lin, M. Elisa Crestoni, S. Fornarini, P. M. Mayer, *J. Mass Spectrom*. 2011, **46**, 546.
12 M. Schäfer, K. Peckelsen, M. Paul, J. Martens, J. Oomens, G. Berden, A. Berkessel, A. J. H. M. Meijer, *J. Am. Chem. Soc.* 2017,**139**, 5779.
13 J. Martens, J. Grzetic, G. Berden, J. Oomens, *Nat. Commun*. 2016, **7**, 11754.
14 J. Martens, G. Berden, C. R. Gebhardt, J. Oomens, *Rev. Sci. Instrum*. 2016, **87**, 103108.
15 L. MacAleese, P. Maitre, *Mass Spectrom. Rev.*, 2007, **26**, 583.
16 J. Oomens, B. G. Sartakov, G. Meijer, G. von Helden, *Int. J. Mass Spectrom*, 2006, **254**, 1.
17 T. D. Fridgen, *Mass Spectrom. Rev.*, 2009, **28**, 586.
18 N. C. Polfer,J. Oomens, Vibrational spectroscopy of bare and solvated ionic complexes of biological relevance, *Mass Spectrom. Rev.*, 2009, **28**, 468–494.
19 N. C. Polfer, *Chem. Soc. Rev.*, 2011, **40**, 2211.
20 R. C. Dunbar, *Int. J. Mass Spectrom,* **377**, 2015, 159.
21 R. C. Dunbar, Top. Curr. Chem. 2015, **364**, 183.
22 A.M. Rijs, J. Oomens, IR Spectroscopic Techniques to Study Isolated Biomolecules, in Gas-Phase IR Spectroscopy and Structure of Biological Molecules, Book Series: Topics in Current Chemistry-Series, 2015, **364**, 1-42.
23 J. Roithova, *Chem. Soc. Rev*., 2012, **41**, 547.
24. J. Oomens & A. Rijs, Top. Curr. Chem. 2015, **364**, 1.
25 A.A. Makarov, I.Y. Petrova, E.A. Ryabov, V.S. Letokhov, *J Phys Chem A*, 1998, **102**,1438.
26 J. D. Steill and J. Oomens, *J. Am. Chem. Soc.* 2009, **131**, 13570.
27 M. Almasian, J. Grzetic, J. van Maurik, J. D. Steill, G. Berden, S. Ingemann, et al., *J. Phys. Chem. Lett.* 2012, **3**, 2259.
28 M. J. Stipdonk, M. J. Kullman, G. Berden and J. Oomens, *Rapid Commun. Mass Spectrom.* 2014, **28**, 691.
29 K. Peckelsen, J. Martens, L. Czympiel, J. Oomens, G. Berden, D. Gründemann, A. Meijer, M. Schäfer, *Phys. Chem. Chem. Phys.*, 2017, **19**, 23362.
30 M. Cossi, N. Rega, G. Scalmani and V. Barone, *J. Comput. Chem.,* 2003, **24**, 669.
31 J. Tomasi, B. Mennucci, R. Cammi, *Chem. Rev.,* 2005, **105**, 2999.
32 L. Brückmann, W. Tyrra, S. Mathur, G. Berden, J. Oomens, A.J.H.M. Meijer, M. Schäfer, *ChemPhysChem* 2012, **13**, 2037.
33 S. A. McLuckey, D. E. Goeringer, *J. Mass Spectrom.* 1997, **32**, 461.
34 J. Clayden, N. Greeves, S. Warren, P. Wothers, Organic Chemistry, 1st Ed., Oxford University Press, Oxford, UK, 2001, 531.
35 J. K. Martens, J. Grzetic, G. Berden, J. Oomens, *Int. J. Mass Spectrom.* 2015, **377**, 179.
36 M.J. Frisch, G.W. Trucks, H.B. Schlegel, G.E. Scuseria, M.A. Robb, J.R. Cheeseman, G. Scalmani, V. Barone, B. Mennucci, G.A. Petersson, H. Nakatsuji, M. Caricato, X. Li, H.P. Hratchian, A.F. Izmaylov, J. Bloino, G. Zheng, J.L. Sonnenberg, M. Hada, M. Ehara, K. Toyota, R. Fukuda, J. Hasegawa, M. Ishida, T. Nakajima, Y. Honda, O. Kitao, H. Nakai, T. Vreven, J.A. Montgomery Jr., J.E. Peralta, F. Ogliaro, M. Bearpark, J.J. Heyd, E. Brothers, K.N. Kudin, V.N. Staroverov, R. Kobayashi, J. Normand, K. Raghavachari, A. Rendell, J.C. Burant, S.S. Iyengar, J. Tomasi, M. Cossi, N. Rega, J.M. Millam, M. Klene, J.E. Knox, J.B.

Cross, V. Bakken, C. Adamo, J. Jaramillo, R. Gomperts, R.E. Stratmann, O. Yazyev, A.J. Austin, R. Cammi, C. Pomelli, J.W. Ochterski, R.L. Martin, K. Morokuma, V.G. Zakrzewski, G.A. Voth, P. Salvador, J.J. Dannenberg, S. Dapprich, A.D. Daniels, Ö. Farkas, J.B. Foresman, J.V. Ortiz, J. Cioslowski, D.J. Fox, Gaussian 09, Revision D.01, Gaussian Inc., Wallingford, CT, 2009.

37 R. Clint Whaley, A. Petitet, J.J. Dongarra, *Parallel Comput.* 2001, **27**, 3.

38 R.C. Whaley, A. Petitet, *Softw. Pract. Exp.* 2005, **35**, 101.

39 A.D. Becke, *J. Chem. Phys. 2993,* **98**, 5648.

40 S. Grimme, S. Ehrlich, L. Goerigk, *J. Comput. Chem.* 2011, **32**, 1456.

41 T.H. Dunning Jr., *J. Chem. Phys.* 1989, **90**, 1007.

42 N.B. Balabanov, K.A. Peterson, *J. Chem. Phys.* 2005, **123**, 064107.

43 K. Peckelsen, J. Martens, G. Berden, J. Oomens, R. C. Dunbar, A. J. H. M. Meijer, et al., *J. Mol. Spectrosc.* 2017, **332**, 38.

44 H. P. Hratchian and H. B. Schlegel, in *Theory and Applications of Computational Chemistry: The First 40 Years*, Ed. C. E. Dykstra, G. Frenking, K. S. Kim, G. Scuseria (Elsevier, Amsterdam, 2005) 195-249.

45 K. Fukui, *Acc. Chem. Res.*, 1981, **14**, 363.

Table of Contents Graphic and TOC sentence

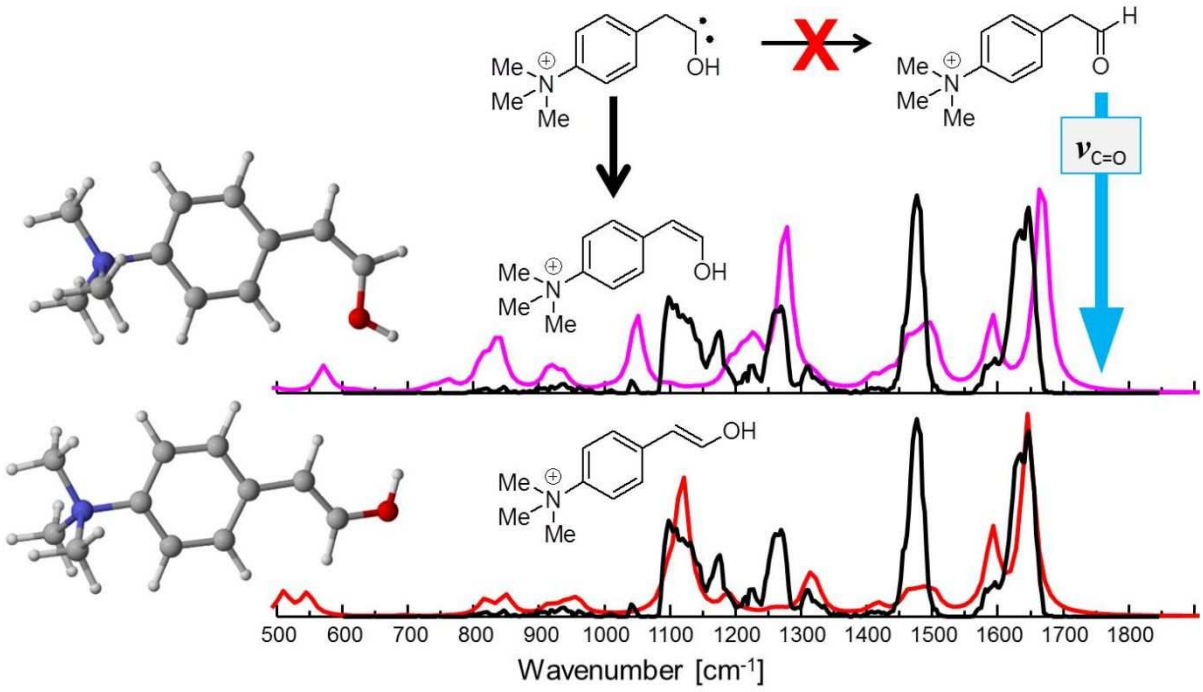

TOC sentence: 19 words (20 words max.)

A charge-tagged hydroxycarbene formed via tandem-MS delivers exclusively enol-tautomers and avoids quantum mechanical hydrogen tunneling in the gas phase.